ELSEVIER

Engineering Structures 21 (1999) 5–15

ENGINEERING STRUCTURES

Some aspects of composite circular sewer linings under installation conditions

M.N. Pavlović,[a] S. Arnaout,[b] S.M. Seraj[c]

[a]*Department of Civil Engineering, Imperial College of Science, Technology and Medicine, London SW7 2BU, UK*
[b]*Technical and Policy Advice Unit to the Ministry of the Environment, PO Box 13-5778, Shouran Post Office, Beirut, Lebanon*
[c]*Department of Civil Engineering, Bangladesh University of Engineering and Technology, Dhaka 1000, Bangladesh*

Received February 1997; revised version accepted June 1997

Abstract

The paper describes the results of both experimental tests and numerical parametric studies aimed at a better understanding of the structural behaviour of closely packed circular-shaped sewer linings. First, the structural responses of complete and segmental linings are compared analytically. Then, vacuum tests carried out on circular glass-reinforced plastic linings to simulate the effect of grouting the annulus gap during installation are reported. Finally, the effect of various restraint conditions, which simulate different temporary support systems that may be used by the contractors during installation of the lining, are investigated; in view of the predominantly membrane response of circular linings to continuous (i.e. flotation and uniform-pressure) loading, approximate design curves, based on a simplified buckling criterion, are presented.

Keywords: Circular sewer linings; Installation conditions; Temporary restraints

Notation

A	dimensionless constants for maximum membrane stress (flotation)
B	dimensionless constants for maximum membrane stress (uniform-pressure)
BC	boundary case
D	diameter of lining
DT	displacement transducer
t	thickness of lining
E_s	allowable short-term modulus of elasticity of lining material
G	unit (specific) weight of grout mix
GRC	glass-reinforced cement
GRP	glass-reinforced plastic
H	excess head of grout (measured from crown of lining) corresponding to uniform-pressure load
I	moment of inertia of lining
K	stiffness of circular lining: $(1/12)(E_s/(1-\nu^2))(t/D)^3$
S	membrane stress at any point in lining
S_{cr}	critical buckling stress
SG	strain gauge
S_t	total membrane stress
p	allowable grouting pressure measured at invert of lining
Q	constant; $(360°/\theta)^2 - 1$
q	uniform-pressure intensity
ν	Poisson's ratio
θ	angle between hinges of arch

1. Introduction

The lining of newly-built or existing sewers of different shapes, apart from improving hydraulic characteristics, leads to the enhancement of the structural capacity of the sewer-soil system. Linings also prevent the sewage and wastewater from escaping into the surrounding soil and, thereby, arrests contamination. The large capital expenditure and the serious traffic disruption during the replacement of existing old sewers can be minimized by the adoption of sewer-lining technology. Linings are usually made of composite materials such as glass-reinforced plastic (GRP) or glass-reinforced cement (GRC). Steel linings are also used. Usually linings take the shape of the existing sewer after allowing for an annulus gap so that the sewer lining fits within the sewer

0141-0296/99/$—see front matter
PII: S0141-0296(97)00135-1

with a roughly uniform gap between the lining and the sewer walls. During installation, the gap between the lining and the sewer is then filled with a cementitious grout which, when set, creates a composite sewer-lining structure.

This aspect of sewer renovation is addressed in the *Sewer rehabilitation manual* [1], with which the first two authors have been involved, and which prompted the research reported in References 2–10. Much of the work focuses on (short-term) installation conditions, although (long-term) operational conditions have also been considered, albeit in less detail. Owing to the varied cross-sectional shapes of existing sewers, a wide range of lining shapes have been studied, including egg-shapes [2–5], inverted egg-shapes [8], horseshoe-shapes [9] and semi-elliptical shapes [10]. One important shape on which data has not yet been made publicly available concerns the circular lining type, and this forms the subject of the present article.

The behaviour of circular sewer linings under various installation and loading conditions is not yet well understood. With this in mind, their structural behaviour is presently studied. Initially, an attempt has been made to compare the structural behaviour of complete and segmental circular linings under hydrostatic pressure. These ring structures are mimicked by a two-dimensional finite-element model, and various packing-off patterns are analysed. Next, vacuum tests conducted on 600 mm diameter circular GRP linings, using different restraint systems, are reported. Finally, extensive numerical parametric studies, conducted in an effort to produce approximate design curves for the rational design of circular sewer linings under uniform-pressure loading, are presented.

2. Comparison of the behaviour of complete and segmental circular linings

2.1. Background

A two-dimensional finite-element program is used to compare the relative structural behaviours of complete and segmental circular linings. The ring is taken as being subjected to full hydrostatic pressure. In this way, various packing-off patterns at different locations around the ring are analysed. Due to the symmetry in both loading and geometry, only half of the ring cross-section is analysed. The elements used in the analysis are two-noded beam elements each having three degrees-of-freedom (horizontal and vertical displacement, and rotation) at each node; a full description of this standard element can be found in the finite-element library background of FINEL [11], the software code employed. The half of the lining is discretized into 20 beam elements of equal length (see Fig. 1). At the appropriate node location, the physical restraints are modelled by fully constraining the two nodal-displacement components, while, at symmetry locations, the relevant (i.e. horizontal) displacement component and the rotational degree-of-freedom are suppressed. A triangular loading is applied throughout the depth of the ring in order to simulate full hydrostatic pressure (flotation load). The specific gravity of the grout is assumed to be 1.68.

The three different packing-off patterns considered in the investigation are shown in Fig. 2. In the first type of boundary condition (Fig. 2a, b), the crown of the lining is restrained from vertical and horizontal movement. It is to be noticed here that, normally, grout is injected through the invert (bottom) of the lining. As grout moves forward and upward during the injection of grout, this may cause the lining to go upward and thereby reduce the annulus gap between the sewer and the lining. This is why a restraint at the crown is always expected. In the second type of boundary condition (Fig. 2c, d), restraints are placed at the crown and at points making an angle of 45° on either side of the crown. Fig. 2e, f show the third type of boundary condition where packing has been provided only at the two points which are located at an angle of 45° on either side of the crown. These boundary conditions (packing-off patterns) are simulated in the analyses by fixing the two displacement components at the relevant nodes. Here, while Fig. 2a, c and e refer to complete circular lining cases a, c and e, Fig. 2(b, d and f) refer to segmental circular lining cases b, d and f. For the segmental case study a pin element

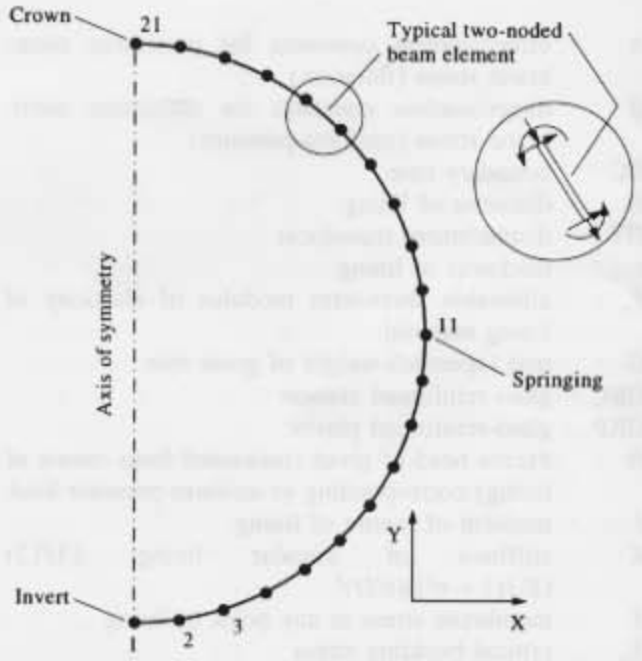

Fig. 1. Circular-shaped lining: two-dimensional finite-element mesh adopted in the analysis.

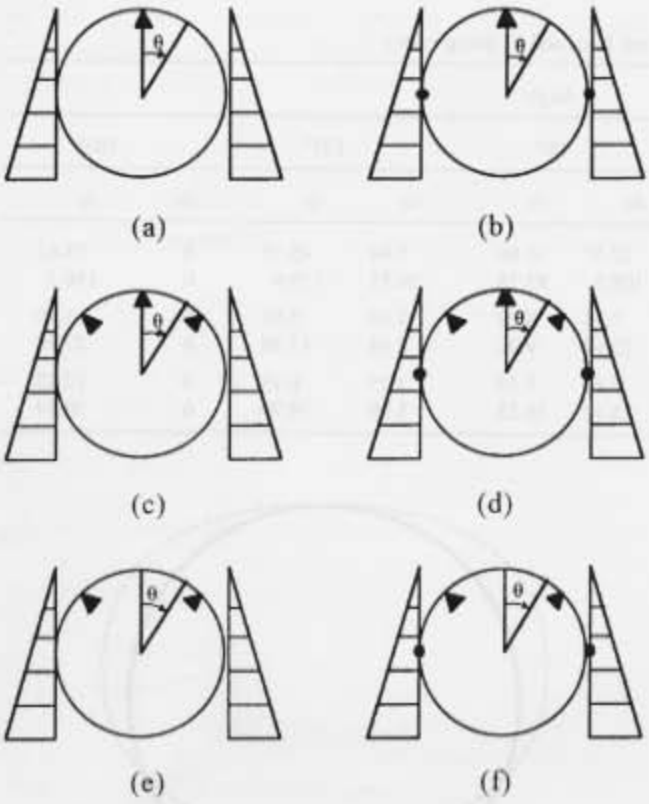

Fig. 2. Circular-shaped lining: various packing-off patterns of complete (a, c, e) and segmental (b, d, f) linings (solid triangles are packing and solid circles are pin elements).

is introduced at the springing level, as shown in Fig. 2b, d, f.

In comparing the behaviour of complete and segmental linings, the material and physical properties of a certain 500 mm diameter and 3 mm thick GRP pipe have been used. The circumferential bending modulus, Poisson's ratio and moment of inertia of the lining used in the analyses are 27777.77 N/mm^2, 0.3 and 2.25 mm^4/unit length (mm), respectively. These values were taken from among typical data provided by manufacturers. For present purposes, where a comparative study of complete and segmental linings under various types of restraint is aimed at, the actual values of material properties for specific linings is not needed. However, it is worth mentioning that manufacturers' data often encompasses a wide range of material values and, in considering a given structure, material tests may need to be carried out. Such material testing (for both bending and axial stiffness) has been described in References 2–4, 12 where detailed accounts of both testing techniques and actual material data can be found. In addition, the possibility of anisotropy in composite linings, such as those made of GRP or GRC, might have to be addressed in three-dimensional structures [7,12]. In fact, GRP linings can be either isotropic or anisotropic [2,3,7,12], but in the present work the former types are considered, although the results can equally be extended to non-isotropic ones because of the essentially two-dimensional nature of the structure owing to the closely-packed restraints (the material properties in the (stiffer) hoop direction are, of course, relevant).

The ensuing values of bending moment and deflection for complete and segmental linings having various restraint conditions, as shown in Fig. 2, are listed in Tables 1 and 2, respectively. In addition, a comparison of the moment diagrams and deflected shapes for cases a and b is shown in Figs. 3 and 4, respectively. The results of the finite-element study permit several useful conclusions to be drawn concerning the relative values of moments and deflections in the ring.

2.2. *Findings of the comparative study*

From a study of cases a and b, it emerges that the value of maximum moment for the segmental lining is about 1.5 times the corresponding maximum moment for the complete case. Both these extreme values occur at the crown of the pipe. An inspection of cases c and d reveals that the value of maximum moment for the segmental lining is about twice the corresponding maximum moment for the complete lining. In these cases, maximum values of moment occur at points located at an angle of 45° from the crown. In cases e and f, the conclusions for cases c and d apply also.

Similarly, from a comparison of cases a and b, it can be seen that the value of the maximum deflection for the segmental lining is 2.6 times the corresponding maximum deflection for the complete lining. Both these values occur at the invert of the pipe. Cases c and d show that the maximum deflection for the segmental lining is 2.4 times the corresponding maximum deflection for the complete lining type. Once again, these values are located at the invert of the pipe. In cases e and f, the findings for cases c and d are also applicable. Finally, Tables 1 and 2 show that, by packing-off the lining at an angle of 45° from the crown (in addition to the pack-

Table 1
Values of moment for the complete (case a, c and e) and segmental (case b, d and e) lining (N.mm/mm)

Case	Angle				
	0°	45°	90°	135°	180°
a (Fig. 2a)	191.5	−40.7	−73.4	11.8	64.4
b (Fig. 2b)	283.3	36.7	0	94.8	151.0
c (Fig. 2c)	17.3	56.1	−32.1	−2.3	27.3
d (Fig. 2d)	34.92	115.2	0	18.2	42.7
e (Fig. 2e)	−14.4	52.4	−33.8	−1.9	28.5
f (Fig. 2f)	−30.0	112.5	0	20.7	46.4

Table 2
Values of displacement for the complete (case a, c and e) and segmental (case b, d, and f) lining (mm)

Case	Angle									
	0°		45°		90°		135°		180°	
	dx	dy	dx	dy	dx	dy	dx	dy	dx	dy
a (Fig. 2a)	0	0	13.45	26.80	27.37	35.66	7.94	45.15	0	59.62
b (Fig. 2b)	0	0	26.05	49.31	108.5	83.78	20.51	119.6	0	156.3
c (Fig. 2c)	0	0	0	0	7.35	3.22	3.10	5.93	0	11.70
d (Fig. 2d)	0	0	0	0	25.64	9.01	5.48	17.56	0	27.50
e (Fig. 2e)	0.70	0.70	0	0	7.87	3.55	3.25	6.45	0	12.47
f (Fig. 2f)	0	0	0	0	28.42	10.23	5.99	19.70	0	30.54

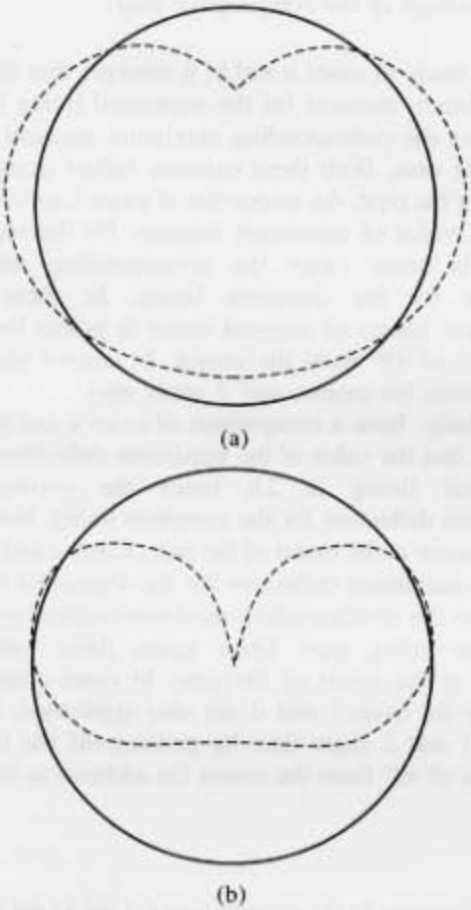

Fig. 3. Circular-shaped lining: moment diagram for (a) complete lining of case a and (b) segmental lining of case b.

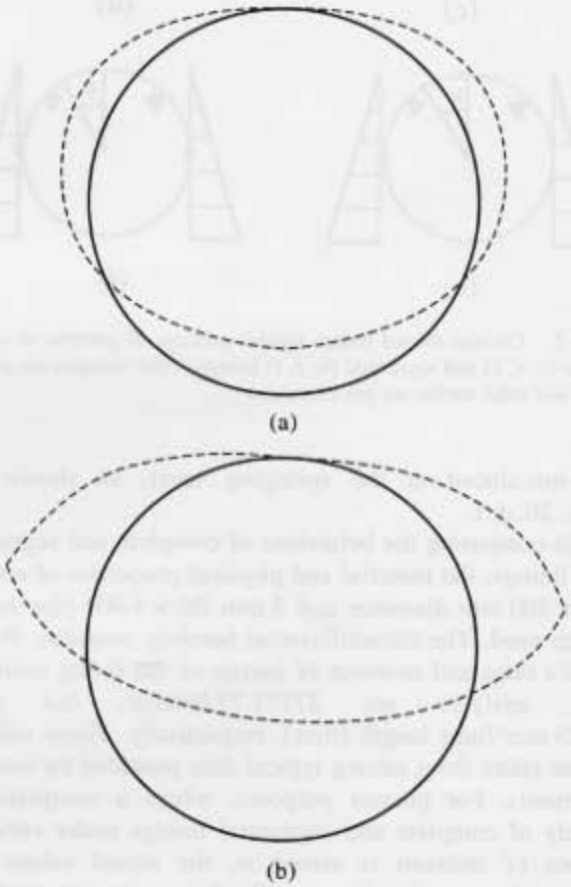

Fig. 4. Circular-shaped lining: deflected shape for (a) complete lining of case a and (b) segmental lining of case b.

ing at the crown), reduces considerably the values of maximum moment and deflection.

3. Vacuum tests on a circular GRP lining

A series of four vacuum tests were carried out on a circular GRP sewer lining, having 600 mm diameter, 7 mm thickness and 2400 mm length, so as to simulate conditions akin to grouting the surrounding annulus during installation. The stiffness of the lining, as provided by the manufacturer, was 1500 N/m^2.

3.1. Restraint systems

The three restraint systems used for the vacuum tests are shown in Figs. 5a–c; Fig. 5d depicts the unrestrained

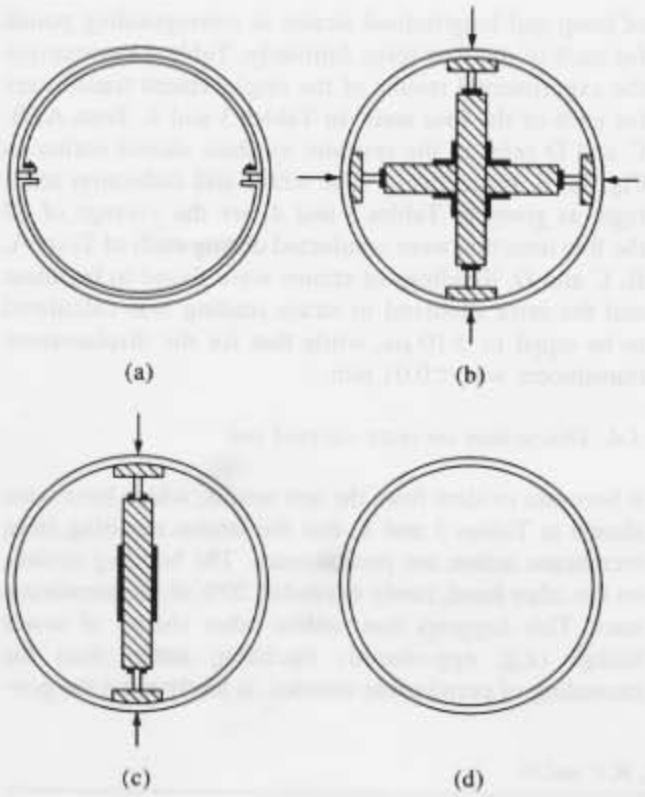

Fig. 5. Circular-shaped lining: restraint systems used in the vacuum tests: (a) steel rings, (b) pair of wooden segments, (c) single wooden segment and (d) unrestrained lining.

case. The first restraint system (Fig. 5a), is made of two semicircular mild-steel rings. These are 50.80 mm wide and 4.76 mm thick. The classical critical buckling pressure for the rings is calculated to be equal to 220 kN/m^2 incorporating a factor of safety equal to 2. The second restraint system (Fig. 5b), consists of two wooden segments fixed to each other in a cross shape. The cross-sectional dimension of each segment is 50 mm × 50 mm and the Euler-column critical buckling load is equal to 0.8 kN including a factor of safety equal to 2. The third restraint system (Fig. 5c) is similar to the second restraint system, except that one wooden segment is used instead of two. During the tests, external clamps were adjusted to give full restraint against displacement at the corresponding points restrained by the wooden segments for both cases.

The restraints were positioned at 600 mm from both ends. The strains induced while adjusting the restraints were monitored and kept as uniform and as low as possible. These strains were measured at a section 1200 mm from the ends and were positioned as shown in Fig. 6a.

3.2. Instrumentation and preparation

Large strain gauges provide improved heat dissipation because they introduce, for the same nominal gauge resistance, lower wattage per unit of grid area. This consideration is important when the gauge is installed on plastics with poor heat-transfer capability. Inadequate heat dissipation causes high temperatures in the grid, backing, adhesive and test-specimen surface, and may noticeably affect gauge performance and accuracy. For this reason, 20 strain gauges of 30 mm length were used and installed on the inner and outer surfaces of the middle section of the lining as shown in Fig. 6a. Four longitudinal strain gauges were installed at the inner and outer surfaces of the liner at points 4 and 9 (see Fig. 6a). The lead wires were connected into terminal blocks, which had been glued to the inside of the lining and were then connected to a cable which passed through a hole drilled in the lining. Half-inch plywood formers were fitted at each end in order to maintain the original cross-sectional shape. The 2400 mm long cylinder was

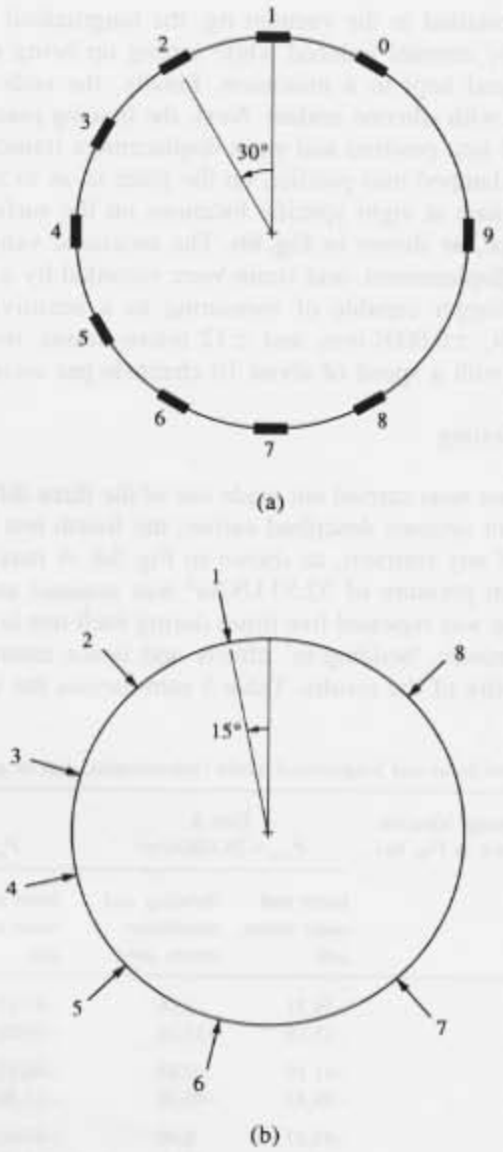

Fig. 6. Circular-shaped lining: (a) strain-gauge locations; and (b) displacement-transducer locations adopted in the vacuum tests.

then installed in the vacuum rig, the longitudinal compressive stresses induced while setting up being monitored and kept to a minimum. Finally, the ends were sealed with silicone sealant. Next, the bracing plate was moved into position and eight displacement transducers were clamped into position on the plate so as to record deflections at eight specific locations on the surface of the pipe, as shown in Fig. 6b. The measured values of load, displacement, and strain were recorded by a computer logger capable of measuring to a sensitivity of ±0.1 N, ±0.0001 mm, and ±12 micro-strains, respectively, with a speed of about 10 channels per second.

3.3. Testing

The four tests carried out made use of the three different restraint systems described earlier, the fourth test being free of any restraint, as shown in Fig. 5d. A maximum vacuum pressure of 32.53 kN/m^2 was attained and the loading was repeated five times during each test in order to eliminate 'bedding-in' effects and hence ensure the reliability of the results. Table 3 summarizes the values of hoop and longitudinal strains at corresponding points for each of the four tests. Similarly, Table 4 summarizes the experimental results of the displacement transducers for each of the four tests. In Tables 3 and 4, Tests A, B, C and D refer to the restraint systems shown earlier in Fig. 5a–d, respectively. The strain and deflection readings, as given in Tables 3 and 4, are the average of all the five tests that were conducted during each of Tests A, B, C and D. Readings of strains were found to be linear and the error involved in strain reading was calculated to be equal to ±10 μs, while that for the displacement transducers was ±0.01 mm.

3.4. Discussion on tests carried out

It becomes evident from the test results, which have been shown in Tables 3 and 4, that the strains resulting from membrane action are predominant. The bending strains, on the other hand, rarely exceeded 20% of the membrane ones. This suggests that, unlike other shapes of sewer linings (e.g. egg-shaped) buckling, rather than the exceeding of permissible stresses, is likely to be the gov-

Table 3
Values of hoop and longitudinal strain (microstrains, μm or μs) for tests A, B, C and D

Strain gauge location (as shown in Fig. 6a)	Test A P_{avg} = 28.10kN/m^2		Test B P_{avg} = 32.26 kN/m^2		Test C P_{avg} = 32.48 kN/m^2		Test D P_{avg} = 32.32 kN/m^2	
	Inner and outer strain, μm	Bending and membrane strain, μm	Inner and outer strain, μm	Bending and membrane strain, μm	Inner and outer strain, μm	Bending and membrane strain, μm	Inner and outer strain, μm	Bending and membrane strain, μm
SG-0	−39.31	2.06	−47.17	4.05	−58.07	8.48	−58.42	5.84
(hoop)	−35.18	−37.24	−39.06	−43.11	−41.10	−49.58	−46.73	−52.57
SG-1	−41.10	0.83	−68.52	23.51	−72.52	4.49	−70.42	6.29
(hoop)	−39.43	−40.26	−21.50	−45.01	−63.54	−68.03	−57.84	−64.13
SG-2	−43.17	0.00	−47.01	1.97	−47.07	−5.87	−46.84	3.95
(hoop)	−43.18	−43.17	−43.00	−45.00	−58.81	−52.94	−54.75	−50.79
SG-3	−33.42	5.86	−37.24	2.91	−43.15	−6.85	−31.11	13.78
(hoop)	−45.15	−39.28	−43.06	−40.15	−56.85	−50.00	−58.67	−44.89
SG-4	−39.26	1.47	−43.01	1.00	−52.95	−17.72	−54.69	9.77
(hoop)	−36.31	−37.78	−45.00	−44.00	−17.51	−35.23	−35.44	−44.91
SG-5	−54.86	7.74	−56.77	10.76	−64.71	6.87	−54.72	7.83
(hoop)	−39.38	−47.12	−35.24	−46.00	−50.97	−57.84	−39.05	−46.88
SG-6	−55.25	10.89	−60.69	13.70	−76.47	20.58	−76.27	20.57
(hoop)	−33.46	−44.35	−33.29	−47.00	−35.30	−55.88	−35.13	−55.70
SG-7	−37.36	7.79	−45.05	0.95	−56.87	20.58	−31.44	5.92
(hoop)	−52.94	−45.15	−46.96	−46.00	−15.71	−36.29	−42.98	−37.06
SG-8	−50.95	5.78	−47.00	2.98	−52.95	4.94	−66.51	7.98
(hoop)	−39.38	−45.16	−41.03	−44.01	−43.06	−48.00	−50.55	−58.53
SG-9	−43.00	5.84	−48.80	18.51	−43.04	12.72	−58.50	15.75
(hoop)	−31.32	−37.16	−11.77	−30.28	−17.60	−30.32	−26.99	−42.75
SG-4	−43.16	5.79	−50.93	8.82	−21.58	10.78	−31.11	9.87
(longitudinal)	−31.58	−37.37	−33.28	−42.10	−43.14	−32.36	−50.85	−40.98
SG-9	−41.19	2.01	−19.61	8.75	−15.70	16.61	−23.41	3.81
(longitudinal)	−37.16	−39.17	−37.11	−28.36	−48.92	−32.31	−31.04	−27.23

Table 4
Values of displacement for tests A, B, C and D

Transducer location (as shown in Fig. 6b)	Test A $P_{avg} = 28.10$ kN/m^2 Displacement, mm	Test B $P_{avg} = 32.26$ kN/m^2 Displacement, mm	Test C $P_{avg} = 32.48$ kN/m^2 Displacement, mm	Test D $P_{avg} = 32.32$ kN/m^2 Displacement, mm
DT-1	–0.02	–0.05	–0.02	–0.05
DT-2	–0.15	–0.09	–0.09	–0.17
DT-3	–0.23	–0.26	–0.16	–0.05
DT-4	–0.14	–0.14	–0.23	–0.22
DT-5	–0.22	–0.09	–0.23	–0.25
DT-6	–0.11	0.02	–0.09	–0.09
DT-7	0.17	0.25	0.33	0.31
DT-8	0.18	0.02	0.07	0.69

erning criterion for the design of circular linings even when the applied pressure is not exactly the uniform one implicit in the vacuum tests (e.g. flotation load). It appears that the restraint systems provided only a relatively minor contribution to the reduction of stresses/strains in the lining since, as a result of these restraints, the values of membrane strains and displacements were usually only slightly reduced; this, too, is in contrast with the case of, say, egg-shaped sewer linings where the governing (predominantly bending) strains are more susceptible to systems of intermediate restraints [2,3].

4. Two-dimensional parametric study of the buckling of large-diameter circular linings

A two-dimensional finite-element program is used to study the structural behaviour of large-diameter circular linings (i.e. 1–2.5 m) subjected to hydrostatic grout pressure. Unlike egg-shaped and inverted egg-shaped linings where bending was found to be predominant [4,8], the vacuum-test results described earlier indicate clearly that buckling due to membrane stresses is to be considered as the likely critical design criterion for circular linings.

The present study assumes that the lining is restrained at different locations around its circumference, and that it behaves as a long cylinder with closely-spaced packing patterns [1]. These restraints consist of hardwood wedges packed at different locations around the cross-section of the lining on the outside, together with internal struts positioned at the same locations. It is assumed that the packing between the sewer and the lining is closely spaced (typically, not exceeding 1–1.5 m spacing), so that the structure can be studied by means of a two-dimensional finite-element model. In this analysis, a dimensionless equation is derived for each boundary case, thus providing a value of critical grouting pressure which can be applied on a particular lining during installation. This value is based on a direct-stress limit criterion which is equal to the critical buckling stress of a hinged arch of similar radius and unrestrained length. A comparison between the different boundary cases is discussed with special emphasis on the enhancement in the values of buckling pressures. Finally, one should mention that staged grouting is not included in this analysis since bending, and not buckling, of the lining is the critical factor which governs design under such loading.

4.1. The two-dimensional model

Due to symmetry about the vertical axis, of both the geometry and the loading configuration, only half of the cross-section of the lining is analysed. This part of the structure is divided into 24 beam elements. The three boundary cases considered in the analysis are shown in Fig. 7. The first boundary case consists of restraints at the crown and invert of the lining (see Figs. 5c and 7a), while the second boundary case adopts restraints at the crown, invert and springings (see Figs. 5b and 7b). The third boundary case consists of restraints at every 45° around the circumference of the lining (see Fig. 7c). The hydrostatic grout pressure which is applied on the lining during the grouting operation can be divided into a linear and a uniform load component. As a result, two loading configurations are included in this analysis, the first one corresponding to a head of grout equal to the crown height as shown in Fig. 8a. This load configuration simulates the flotation pressure which is applied on the lining during grouting. The second load configuration corresponds to uniform pressure applied on the lining due to an excess head of grout as shown in Fig. 8b. As mentioned above, these two load configurations can be superimposed in order to simulate the grout pressure applied on the lining during full grouting. The geometrical parameters D and t, material parameters E_s and ν, and loading parameters G and H have been used in the analysis. These parameters have been defined under Notation.

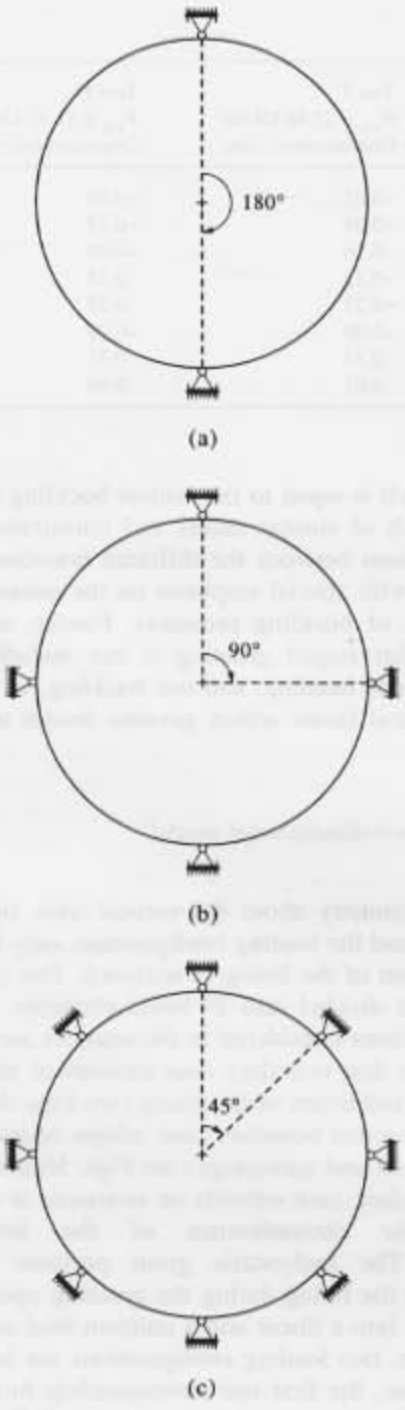

Fig. 7. Circular-shaped lining: (a) boundary case 1; (b) boundary case 2; and (c) boundary case 3 used in the parametric study.

4.2. The dimensionless equations

Once a load configuration is chosen and a boundary case is selected the parametric study is carried out by varying one parameter at a time while keeping the others constant. At the end, a dimensionless equation is derived linking all the independent parameters together.

In order to consider subsequently buckling in the analysis, dimensionless equations for the membrane stress S at any point in the lining are obtained for the two loading cases of flotation and uniform pressure, as follows:

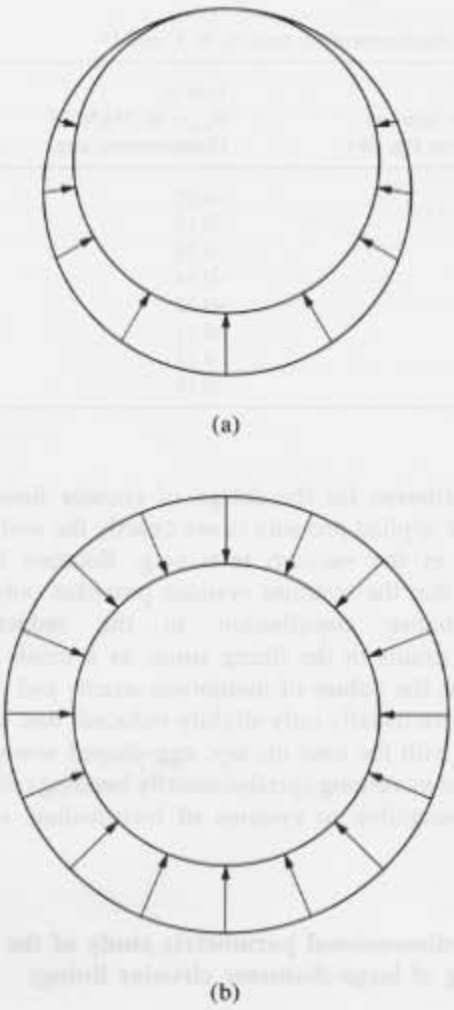

Fig. 8. Circular-shaped lining: (a) flotation; and (b) uniform pressure load configurations adopted in the parametric study.

(a) Flotation

$$S/GD = A(D/t) \quad (1)$$

(b) Uniform pressure

$$S/GD = B(D/t)(H/D) \quad (2)$$

where A and B are constants which depend on the boundary case adopted during grouting.

The total direct membrane stress (S_t) at any point in a lining subjected to a head of grout which is greater than the lining height D (i.e. full grouting), can be divided into values of membrane stresses resulting from each of the flotation loading and the uniform pressure. This leads to the following dimensionless equation for the total membrane stress in the lining:

$$(S_t/GD)(t/D) = (A + B(H/D)) \quad (3)$$

As the point of injection of the grout is usually located at the invert of the lining, the value of H in equation (3) can conveniently be replaced by the equivalent expression of $(p/G - D)$ where p is the allowable grouting pressure measured at the invert of the lining. In the end, equation (3) can be re-written so as to yield the following generic design equation for the different boundary conditions of interest:

$$(S_t/GD)(t/D) = (A - B + B(p/GD)) \quad (4)$$

The critical buckling stress due to membrane action S_{cr} of a hinged arch of equivalent radius and unrestrained length is given by the following equation [13]:

$$(S_{cr}/GD)(t/D) = 4.0(K/GD)Q \quad (5)$$

where K is the stiffness of the circular lining, i.e.

$$K = (1/12)(E_s/(1 - \nu^2))(t/D)^3 \quad (6)$$

where Q in equation (5) is a constant which depends on the angle θ between the hinges of the arch and is expressed as follows:

$$Q = (360°/\theta)^2 - 1 \quad (7)$$

Equating equations (4) and (5) and using the appropriate value of Q from equation (7) leads to a general design equation for the critical buckling pressure given by

$$(K/GD)(4Q) = A - B + B(p/GD) \quad (8)$$

4.3. Construction of design curves

As mentioned earlier, for each load and boundary case, the parametric analysis is carried out by varying one parameter at a time, keeping the others unchanged. Thus, axial stresses are given in terms of dimensionless equations linking all the independent parameters together. The non-dimensional membrane stress (S/GD) is plotted against (D/t) and $(D/t)(H/D)$, for the flotation loading and the uniform-pressure case, respectively. From these plots, constants for the maximum membrane stress in the lining are computed for the different boundary cases and the different loading configurations. The values of the dimensionless constants A and B at the location of maximum membrane stress, as obtained from the resulting extensive parametric study, are listed in Table 4. Using equation (7), the values of Q for each of the three boundary cases 1, 2 and 3 shown in Fig. 7 are readily obtained as 3, 15 and 63, respectively. The ensuing design curves appear in Fig. 9.

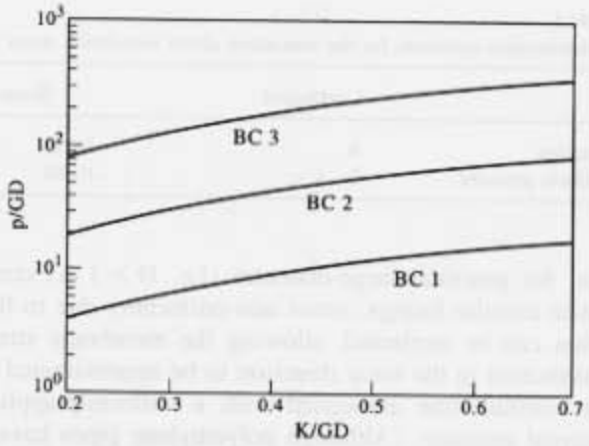

Fig. 9. Circular-shaped lining: critical value of grouting pressure based on buckling criteria for various boundary conditions.

4.4. Discussion of the buckling analysis

It is evident from equation (4) in conjunction with Table 5 that the value of the maximum membrane stress in the lining is not reduced considerably when additional restraints are introduced. However, the effective length of the arch between the restraints is reduced, thus leading to a stiffer structure with higher critical buckling pressure. On the other hand, it must be noted that the assumption of an equivalent hinged arch is conservative and can be considered as a lower-bound solution since the structural behaviour of the portion of the lining which initiates buckling (and hence is taken as the critical portion) lies between a hinged and a fixed arch. It is worth mentioning that the critical buckling pressure of a fixed arch can reach two to six times the value of a hinged arch [6] for boundary cases 2 and 3, respectively.

However, the variation of membrane stress values around the circumference of the lining is gradual, so that the restraint provided by the arch portions adjacent to the critical one is relatively small and, hence, a hinged condition for the latter seems to provide a reasonable assumption. For the extreme case of non-uniform loading (i.e. flotation pressure), the ratio of membrane stresses between the most stressed and least stressed regions can be large depending on the boundary condition used during installation (i.e. 1.5 for boundary condition 1, 4.5 for boundary condition 2 and 17.5 for boundary condition 3) and this fact highlights the need for the finite-element analysis in order to identify the critical arch portion of the lining. On the other hand, if the head of grout is large, a reasonably uniform state of compression can be assumed around the circumference and all arch portions are expected to initiate buckling almost simultaneously. Now, by reference to Fig. 9, it is clear that, for the range of lining types (as described by K/GD) presently considered, buckling is unlikely to occur below a grouting pressure equivalent to at least four times the diameter (i.e. $p/GD > 4$); this suggests

Table 5
Dimensionless constants for the maximum direct membrane stress in the lining

	Coefficient	Boundary case 1		Boundary case 2		Boundary case 3	
Flotation	A	−0.293	node 1	−0.400	node 1	−0.452	node 1
Uniform pressure	B	−0.498	constant	−0.498	constant	−0.482	constant

that, for practical large-diameter (i.e. $D > 1$ m) composite circular linings, stress non-uniformity due to flotation can be neglected, allowing the membrane stress distribution in the hoop direction to be approximated to the constant one associated with a uniformly-applied external pressure. (Although polyethylene pipes have a considerably lower K when compared to most other linings, their large thickness and relatively low diameter (not exceeding 1 m) [1], as well as their method of installation, rule them out of present considerations.)

By comparing the three boundary cases used in the analysis with the case of an unrestrained circular pipe, it can be concluded that, only when boundary cases 2 and 3 are adopted as restraint set-ups during installation, the value of the critical buckling pressure of the circular lining increases considerably (the unrestrained case is not actually shown in Fig. 9 since it differs negligibly from boundary case 1). Hence the enhancement factors resulting from boundary cases 2 and 3 (with respect to boundary case 1 which is taken as the datum) are of the order of 5 and 20, respectively. However, in view of the uncertainty regarding imperfection sensitivity in the buckling of circular linings (imperfection insensitivity was assumed in the present analysis, following the works of Budiansky [14] and Carrier [15], but their findings are contradicted by Rehfield [16]), it may be advisable to somewhat reduce these enhancement factors.

5. Conclusions

The present report on a series of short, and perforce limited, studies aimed at exploring some structural aspects of composite circular sewer linings during installation has yielded the following, albeit tentative, conclusions.

A two-dimensional numerical parametric study focusing on the flotation loading has shown that both moments and deflections induced in a segmental circular lining are much higher than their corresponding values in a complete (i.e. single-unit) lining. This confirms that complete sewer linings have considerable structural advantages when compared to segmental ones.

Vacuum tests on circular linings have shown that, under-uniform pressure conditions, the values of the bending strains are a very small fraction of their membrane counterparts. This indicates that the initial imperfections, which give rise to these bending effects are quite small, and can be neglected for elastic working-stress analysis. Unlike non-circular (e.g. egg-shaped) linings, allowable (bending) stresses/strains are not likely to be the design criterion, nor do intermediate restraints play an important role. (Bending, however, may be more relevant for non-uniform pressure conditions, such as partial or full grouting; in this respect, the present tests provide a useful benchmark for three-dimensional finite-element analysis of circular sewer linings along the lines adopted for egg-shaped pipes, as described in Reference 7.) Therefore, in view of the predominantly membrane response of circular linings to uniform-pressure loading, buckling is in fact likely to be the governing criterion for their design.

A two-dimensional numerical parametric study shows that restraints in circular linings do not reduce appreciably the membrane stresses. Nevertheless, additional restraints lead to a stiffer structure with higher critical buckling pressures. A simplified buckling estimate enables approximate design curves to be derived for various restraint systems, and covering simultaneously both flotation and uniform-pressure (i.e. additional head) loading conditions: an inspection of these curves indicates that buckling is unlikely to give rise to concern unless a considerable head of grout (additional to, and well exceeding, flotation) is applied during installation, implying that the non-uniformity of membrane stresses due to the flotation component can be neglected.

Acknowledgements

The material in this paper is largely based on two earlier reports prepared for WRc Engineering, whose financial support for this work is gratefully acknowledged. Thanks are also due to Dr G. M. A. Jones and Dr J. W. Dougill for helpful technical discussions.

References

[1] Water Research Centre. Sewerage rehabilitation manual, Swindon, 1983.

[2] Arnaout S, Pavlović MN. The structural behaviour of egg-shaped sewer linings with special emphasis on their current problems and research. In: Non-Conventional Structures (Proc Int Conf Design and Construction of Non-Conventional Structures), London, Topping BHV, editor, Civil-Comp Press, Edinburgh, 1987;2:231–38.

[3] Arnaout S, Pavlović MN. Studies on the structural behaviour of

egg-shaped sewer linings under installation and operational conditions. Struct Engng Rev 1988;1:25–33.
[4] Arnaout S, Pavlović MN, Dougill JW. Structural behaviour of closely packed egg-shaped sewer linings during installation and under various restraint conditions. Proc ICE (Part 2) 1988;85:49–65.
[5] Arnaout S, Pavlović MN. An investigation into the long-term behaviour of egg-shaped sewer linings. In: Foundations and Tunnels – 89 (Proc Second Int Conf on Foundations and Tunnels). London (Forde MC, editor, Engineering Technics Press), Edinburgh, 1989;2:207–13.
[6] Arnaout S, Pavlović MN, Dougill JW. A new method for testing the tensile properties of curved specimens. Mater Struct RILEM 1990;23:296–304.
[7] Pavlović MN, Arnaout S, Hitchings D. Finite element modelling of sewer linings In: Developments in Structural Engineering Computing (Proc Fifth Int Conf on Civil and Structural Engineering Computing, CIVIL-COMP 93), Edinburgh, Topping BHV, editor, Civil-Comp Press, Edinburgh, 1993, D, 1–11 (Reprinted with small additions) in Comput Struct 1997;63:837–48).
[8] Seraj SM, Roy UK, Pavlović MN. Structural behaviour of closely packed inverted egg-shaped sewer linings during installation and under various restraint conditions. Thin-Walled Struct (in press).
[9] Seraj SM, Roy UK, Pavlović MN. Structural design of closely packed horseshoe-shaped sewer linings during installation. Thin-Walled Struct (in press).
[10] Seraj SM, Roy UK, Pavlović MN. Semielliptical-shaped sewer linings under installation conditions (submitted).
[11] Hitchings D. FINEL, Aeronautics Department, Imperial College, London, 1983.
[12] Arnaout S. The structural performance of egg-shaped sewer linings. PhD thesis, University of London, 1988.
[13] Thimoshenko SP, Gere JM. Theory of elastic stability, McGraw-Hill, New York, 1961.
[14] Budiansky B. Theory of buckling and postbuckling behaviour of elastic structures. J Adv Appl Mech 1974;14:1–65.
[15] Carrier GF. On the buckling of elastic rings. Math Phys 1947;26:94–103.
[16] Rehfield LW. Initial post buckling of circular rings under pressure loads. AIAA Journal 1975;10:1358–59.